remote sensing

MDPI

Article

Potential Impact of Sea Surface Temperature Variability on the 2007 Sudden Bloom of *Ulva prolifera* in the Southern Yellow Sea

Yufeng Pan [1,2], Pin Li [3,*], Jiaxuan Sun [4], Siyu Liu [1,5], Lvyang Xing [1,2], Di Yu [1,2] and Qi Feng [1,2]

1 Key Laboratory of Submarine Sciences and Prospecting Techniques, Ministry of Education of the People's Republic of China, Ocean University of China, Qingdao 266100, China; panyufeng@stu.ouc.edu.cn (Y.P.); 11220411020@stu.ouc.edu.cn (S.L.); xinglvyang@stu.ouc.edu.cn (L.X.); yuayu@stu.ouc.edu.cn (D.Y.); 21210411048@stu.ouc.edu.cn (Q.F.)
2 College of Marine Geoscience, Ocean University of China, Qingdao 266100, China
3 First Institute of Oceanography, MNR, Qingdao 266100, China
4 Qingdao West Coast New Area Marine Development Bureau, Qingdao 266000, China; sjx1251@stu.ouc.edu.cn
5 Academy of the Future Ocean, Ocean University of China, Qingdao 266100, China
* Correspondence: pinli@fio.org.cn

Abstract: Since 2007, *Ulva prolifera* (*U. prolifera*) originating in northern Jiangsu (NJ) has consistently expanded to the southern coast of the Shandong Peninsula. However, the underlying reasons for the 2007 sudden bloom of *U. prolifera* on a large scale remain unknown. This study uses remote sensing data from MODIS/AQUA spanning the period 2003–2022 to investigate the sea surface temperature (SST) structure changes in the southern Yellow Sea (SYS) over the past 20 years. The results demonstrate the following. (1) Since 2007, the NJ northward current and the Yangtze estuary warm current have exhibited higher temperatures, earlier northward intrusions, and larger influence areas, leading to a faster warming rate in NJ before mid-May. This rapid increase in SST to a level suitable for early *U. prolifera* growth triggers large-scale blooms. (2) The change in temperature structure is primarily induced by a prolonged and intense La Niña event in 2007–2008. However, since 2016, under stable global climate conditions, the temperature structure of the SYS has returned to the pre-2007 state, corresponding to a decrease in the scale of *U. prolifera* blooms.

Keywords: *Ulva prolifera*; sea surface temperature; Northern Jiangsu northward current; warm current across the Yangtze River Estuary; MODIS/AQUA

check for updates

Citation: Pan, Y.; Li, P.; Sun, J.; Liu, S.; Xing, L.; Yu, D.; Feng, Q. Potential Impact of Sea Surface Temperature Variability on the 2007 Sudden Bloom of *Ulva prolifera* in the Southern Yellow Sea. *Remote Sens.* **2024**, *16*, 4407. https://doi.org/10.3390/rs16234407

Academic Editor: Chung-Ru Ho

Received: 26 September 2024
Revised: 18 November 2024
Accepted: 19 November 2024
Published: 25 November 2024

Copyright: © 2024 by the authors. Licensee MDPI, Basel, Switzerland. This article is an open access article distributed under the terms and conditions of the Creative Commons Attribution (CC BY) license (https://creativecommons.org/licenses/by/4.0/).

1. Introduction

The green tide has emerged as a significant marine disaster impacting coastal regions worldwide. Investigating the underlying mechanisms contributing to its onset holds crucial practical implications for predicting and mitigating large-scale disasters. Since 2007, the proliferation of *Enteromorpha* in the western region of the southern Yellow Sea (SYS) has resulted in large-scale blooms. This phenomenon has had severe impacts on coastal fisheries and tourism in Jiangsu and Shandong provinces, making it one of the most severe marine disasters in China. The tongue-shaped topography (Figure 1, yellow dashed square) off the coast of northern Jiangsu (NJ) is characterized by extensive shallow waters (particularly the NJ shallow, with depths of less than 20 m), located between the abandoned Yellow River Estuary and the Yangtze Estuary where radial sand ridges spread, creating a significant breeding base for *Porphyra yezoensis*. Previous studies using remote sensing monitoring and homology analysis have indicated that *Enteromorpha* blooms in the SYS predominantly originate along the *Porphyra* aquaculture rafts coast of Jiangsu province [1–3]. Morphological and molecular analyses have revealed five to seven species of attached algae from *Enteromorpha*, including *Ulva Prolifera* (*U. Prolifera*), *Ulva linza*, *Ulva*

compressa, *Ulva intestinalis*, *Ulva flexuosa*, and *Ulva clathrata* [4,5]. The dominant species responsible for these blooms is *U. prolifera* [6,7].

The occurrence of green tide events closely relates to multiple factors [8] including sea surface temperature (SST), nutrient concentrations, and light intensity. In previous research, the primary focus has been the overall oceanographic conditions and their impact on *U. prolifera* within a single year or a relatively short timescale in the SYS [9–14]. Despite the eutrophication status of the SYS, the nutrient concentration remains sufficient for *U. prolifera* to bloom, despite reduced nutrient levels in springtime [15–17]. Analysis of local aquaculture and environmental data strongly suggests that the *U. prolifera* in both the SYS and East China Sea, including massive blooms in the summers of 2008 and 2009, is unlikely to be solely caused by coastal eutrophication [3,15,18]. Therefore, a suitable SST has emerged as the critical factor in the large-scale bloom of *U. prolifera*, with temperatures of 15–25 °C being most favorable for its growth [19]. Laboratory studies have demonstrated that the early growth of *U. prolifera* is more substantial than in other species when the SST reaches 10–20 °C [20]. As for chlorophyll-a concentration, this has a negative correlation with the occurrence of *U. prolifera* in the SYS [21]. Furthermore, the prevailing southeast summer monsoon in the SYS acts as the primary driving force for the northward drift and diffusion of *U. prolifera* [3,22,23]. Hu et al. established a robust relationship to link biomass per area to the reflectance-based floating algae index (FAI) [24]. Since 2007, *U. prolifera* has originated near the NJ shallow from April to May each year, drifting northward to reach its maximum coverage and distribution area in June. Subsequently, the bloom gradually diminishes from July to August along the southern coast of the Shandong Peninsula.

Existing studies have overlooked the relationship between long-term changes in SST structure and the occurrence of *U. prolifera* blooms. Although *U. prolifera* was observed almost every year from 2000–2009, the extent of its coverage before 2008 was considerably smaller than in 2008 and 2009 [18], and there are notable interannual variations in its occurrence. The reasons for the 2007 sudden large-scale blooms have not been thoroughly investigated. Therefore, investigating the underlying mechanisms contributing to its onset holds crucial practical implications for predicting and mitigating large-scale disasters. Our research suggests that, since 2007, *U. prolifera* has originated in NJ during April and May, leading to widespread northward dispersion driven by wind drift and the increasing SST in the SYS [25]. To further explore these changes, remote sensing data from MODIS/AQUA spanning the period from 2003–2022 are used to compare the SST structure before and since 2007. By conducting correlation analyses between SST and the coverage area of *U. prolifera*, this study investigates the effects of temperature structure changes influenced by the current system on the sudden bloom of *U. prolifera* and its intensity.

2. Geological Setting

The study area (Figure 1) is a typical plain siltation coast. In the central and northern expanses of the SYS, the sea plain is wide and shallow, producing a gently contoured sector. This zone is a stable accumulation landform, marked by sediments of a notably fine granularity [26]. The central and southern sectors of the western coastline of the SYS are distinguished by an array of emanating tidal sand ridges, colloquially referred to as the NJ shallow, which extend across an aggregate area of roughly 35,000 square kilometers.

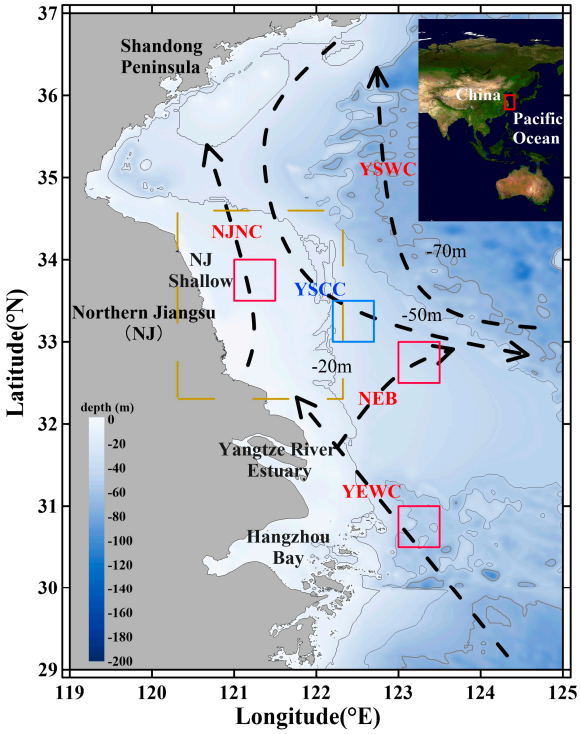

Figure 1. Schematic map of the study area. The black single-arrow dashed curves depict the primary flow paths, as primarily determined by previous studies [27–29] and the temperature structure in Chapter 4.2. The red and blue squares indicate the characteristic regions associated with each respective current. The yellow dashed square is the tongue-shaped topography area where *Ulva prolifera* (*U. prolifera*) originates. The visual representation is rendered using the Surfer16 software.

In the western region of the SYS, where *U. prolifera* blooms occur, there is a marked coastal current. Traditionally, it was believed that the Yellow Sea coastal current (YSCC) originated near Haizhou Bay and flowed southward to the north of the Yangtze River Estuary. The YSCC is formed by the runoff from the Guan River and Sheyang River in NJ, which mixes with coastal seawater. The SST in this region is approximately 28 °C, and the salinity ranges from 28–29 psu [30,31]. However, recent studies based on Argo data and numerical simulations suggest that the YSCC exhibits a northward flow during the summer months, specifically along the NJ northward current (NJNC) region. This northward current aligns with the drift path of *U. prolifera* from the NJ shallow to the southern coast of the Shandong Peninsula [32,33]. Furthermore, preliminary research indicates that the warm current across the Yangtze River Estuary (YEWC), of which the Taiwan warm current is the main component, influences the SST of the SYS during summer [25].

3. Materials and Methods

3.1. Materials

The remote sensing data used in this research consist of SST Level 2 data obtained from the MODIS/AQUA satellite. These data were acquired through NASA's Ocean-Color Web platform (https://oceancolor.gsfc.nasa.gov/, Accessed on 17 October 2022) and were made available with the support of the Ocean Biology Processing Group (OBPG) at NASA's Goddard Space Flight Center. The SST data exhibit a temporal resolution of 1 day and a spatial resolution of 1 km. To assess the reliability and accuracy of the measurements, each pixel in the data was assigned a numeric quality level: 0-BEST, 1-GOOD, 2-QUESTIONABLE, 3-BAD, and 4-NOT PROCESSED.

The nutrient concentrations were taken from the Global Ocean Biogeochemistry Analysis and Forecast (GOBAF) dataset, provided by the EU Copernicus Marine Service In-

formation (https://doi.org/10.48670/moi-00015, Accessed on 15 September 2023). This dataset has a temporal resolution of 1 day and a spatial resolution of 0.25°.

The in-situ SST data used in this study were obtained from multiple sources and were collected using conductivity–temperature–depth measurements with Sea-bird911 instruments. These measurements were taken at depths ranging from 0–5 m. Specifically, a total of 677 in-situ data points were obtained in the SYS region from 2006–2019, as illustrated in Figure 2a.

The supplementary data pertaining to the impacts of *U. prolifera* in this paper were sourced from the *Bulletin of China Marine Disaster* (*BCMD*) [9,34,35]. The *BCMD* is an official publication issued annually by the Ministry of Natural Resources of the People's Republic of China, typically released in March or April each year. It provides comprehensive and detailed records of various aspects related to *U. prolifera* blooms, including the earliest discovery location, maximum distribution date and area (MDA), maximum coverage date and area (MCA), and other relevant parameters. Prior to 2021, the MDA and MCA metrics were identified and monitored using satellite imagery with a resolution of 250 meters. From 2021 onwards, these parameters have been tracked using satellite imagery with an enhanced resolution of 50 meters. These records have been consistently documented since 2009. Additionally, this study references pertinent information from the *Green Tide Remote Sensing Monitoring Bulletin*, published by the National Satellite Marine Application Centre [36].

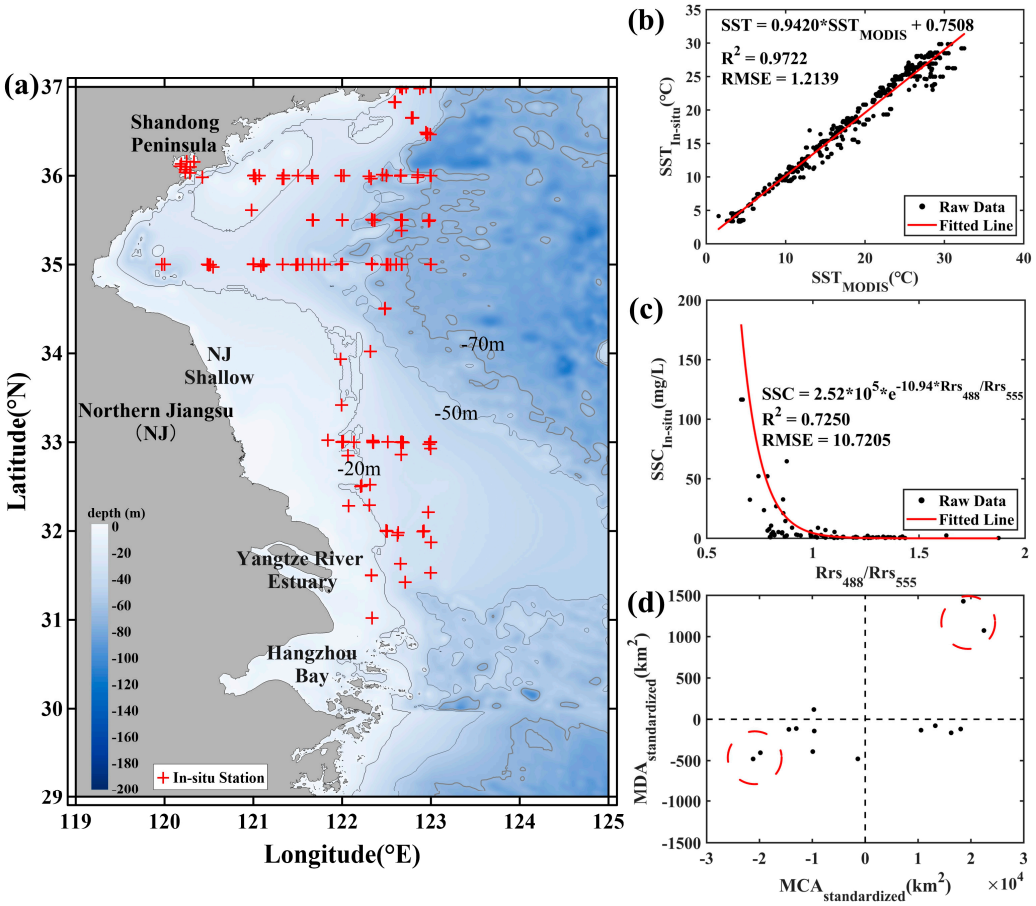

Figure 2. (**a**) Distribution of in-situ data survey stations. (**b**) Correlation analysis between the sea surface temperature (SST) derived from MODIS/AQUA satellite imagery and in-situ data. (**c**) Correlation analysis between the suspended sediment concentration (SSC) derived from MODIS/AQUA satellite imagery and in-situ data. (**d**) Standardized calculation for the classification of the *U. prolifera*.

3.2. Methods

The MODIS/AQUA remote sensing data used in this study were subjected to a series of preprocessing and inversion procedures, involving both data formatting and the utilization of in-situ data for calibration. Poor quality data points (indicated by a quality level greater than 2) were excluded. The inversion process primarily relies on establishing a correlation between the values obtained from in-situ data and the corresponding remote sensing data. By comparing the time, longitude, and latitude of the survey stations, this study identified matching points in the remote sensing data that align with the same time and location, allowing for the retrieval of the corresponding values. This study collected data from a total of 677 in-situ data stations spanning the period from 2006–2019. Among these, 222 stations were successfully matched to the remote sensing data, resulting in the acquisition of 540 valid remote sensing values. When identifying matching points, the observed remote sensing data for the day were used within a circular area with a 1 km radius around the corresponding in-situ station. The high coefficient of the SST inversion formula (Table 1, Equation (1)) determination (R^2) of 0.9722, as shown in Figure 2b, signifies a strong correlation between the in-situ data and the MODIS/AQUA data.

Table 1. Methods and formulas.

Datasets		Methods	Formulas	Parameters	Remarks
MODIS/AQUA data	SST	Inversion	$\mathrm{SST} = 0.942 * \mathrm{SST}_{MODIS} + 0.7508$ (1)		Obtained the spatial pattern of SST during *U. prolifera* bloom events.
		Warming rate (WR)	$WR = \left(X^T X\right)^{-1} X^T t$ (2)	X is the SST of a specific pixel in different time periods; t is the different time periods.	Obtained the speed of SST changes over different time periods.
		Inversion of the suspended sediment concentration (SSC)	$WRA = WR_{mid-May\ to\ late-June} - WR_{early-April\ to\ mid-May}$ (3)		Highlighted the difference in SST changes between the origin and outbreak stage of the *U. prolifera* event.
		The monthly mean value of nutrient concentrations	$\mathrm{SSC} = 2.52 * 10^5 * e^{-10.94 * (\frac{Rrs_{488}}{Rrs_{555}})}$ (4) [37,38]	Rrs_{488} and Rrs_{555} are 488 nm and 555 nm bands, respectively.	Obtained the SSC value and its spatial pattern during *U. prolifera* bloom events.
GOBAF dataset		The monthly mean value of nutrient concentrations	/		Obtained nutrient concentrations including the mole concentrations of nitrate (NO_3), phosphate (PO_4), and silicate (Si) in seawater.
Bulletin of China Marine Disaster (*BCMD*)		Standardized calculation for the classification of the *U. prolifera*	$S = X - \overline{X}$ (5)	S represents the standardized value; X represents the MCA or MDA value of each year; and $\overline{X}$ represents the mean value of the MCA or MDA from 2008–2022.	

Table 1. *Cont.*

Datasets	Methods	Formulas	Parameters	Remarks
/	Pearson product-moment correlation coefficient (PPMCC)	$r(X,Y) = \frac{n\sum_{i=1}^{n} x_i y_i - \left(\sum_{i=1}^{n} x_i\right)\left(\sum_{i=1}^{n} y_i\right)}{\sqrt{n\sum_{i=1}^{n} x_i^2 - \left(\sum_{i=1}^{n} x_i\right)^2}\sqrt{n\sum_{i=1}^{n} y_i^2 - \left(\sum_{i=1}^{n} y_i\right)^2}}$ (6)	X is the SST of a specific pixel and time period, but from different years; Y is the coverage area of *U. prolifera* for the same time period, but from different years (within 2010–2019)	Obtained the spatial pattern of the PPMCC between SST and the coverage area of *U. prolifera* and assessed the extent to which SST impacts *U. prolifera* in different periods and locations.

To obtain the spatial pattern of SST during *U. prolifera* bloom events (from April to August), the inverted SST data were processed using a 10-day average. However, for months containing 31 days, the average for the 11th day was used as the late average for that month. This approach allows for the characterization of the SST spatial patterns in the early, middle, and late periods of each month.

Additionally, the SST for different time series was calculated using the least-squares method to analyze the SST warming rate (WR) (Table 1, Equation (2)). To further analyze the WR difference between different time periods, the WR anomaly (WRA) (Table 1, Equation (3)) was computed by subtracting the WR of the early April to mid-May period (the origin stage of the *U. prolifera* event) from the WR of the mid-May to late June period (the outbreak stage of the *U. prolifera* event). To assess the extent to which the SST impacts *U. prolifera* in different periods and locations, the spatial pattern of the Pearson product-moment correlation coefficient (PPMCC) (Table 1, Equation (5)) between the SST and the coverage area of *U. prolifera* was derived using MODIS/AQUA data and the coverage area data from 2010–2019 [36].

In addition, previous studies [37,38] have demonstrated that the suspended sediment concentration (SSC) can be estimated using the 488 nm (Rrs_{488}) and 555 nm (Rrs_{555}) bands of MODIS/AQUA satellite data. This study collected data from a total of 289 in-situ data stations spanning the period from 2006–2019. Among these, 46 stations were successfully matched to the remote sensing data, resulting in the acquisition of 77 valid remote sensing values. The R^2 of the SSC inversion formula reaches 0.7250, as shown in Figure 2c. The nutrient concentrations considered in this study include the mole concentrations of nitrate (NO_3), phosphate (PO_4), and silicate (Si) in seawater. The data span the period 2003–2020, and the monthly mean values for the study area were calculated. The processing of all nutrient concentration datasets was conducted using MATLAB/2023a.

4. Results

4.1. Impact Factors: Nutrient Concentration, SSC, and SST

4.1.1. Nutrient Concentration and SSC

By processing the GOBAF dataset and inverting the SSC, the monthly spatial averages for the study area were derived (Figure 3). From April to June, the nutrient concentrations remain relatively consistent both before and since the years 2007–2008. The mean and standard deviation ($x \pm s$) before and since 2007 are presented in Table 2. There are only minor changes in nutrient concentrations during these years (Figure 3, blue box). The most substantial alteration pertains to the concentration of PO_4 in the month of June, which increases by 45.28%. Following this increase, the PPMCC between the concentration of PO_4 and the MCA of *U. prolifera* reaches a value of 0.19.

Turbidity refers to the degree of cloudiness or haziness in water caused by suspended particles, which directly influences the availability of light to *U. prolifera* and subsequently impacts its growth [25]. In the study area, the average SSC values for June in the years 2007–2008 are lower than in other periods (Figure 3). However, there is an increasing trend in SSC both before and since 2007–2008. This enhanced turbidity could potentially

attenuate the sunlight intensity, thereby limiting the growth of *U. prolifera*. The PPMCC values between the SSC for April, May, and June and the MCA of *U. prolifera* in different years are −0.05, −0.16, and −0.05, respectively.

Table 2. Statistics of nutrient concentration.

		NO_3 * (mmol/m^3)	PO_4 * (mmol/m^3)	Si * (mmol/m^3)
April	2003–2006	5.73 ± 0.31	0.0093 ± 0.0023	12.43 ± 0.58
	2007–2020	5.64 ± 0.48	0.0093 ± 0.0024	12.91 ± 0.63
May	2003–2006	7.63 ± 0.72	0.0059 ± 0.0009	12.61 ± 0.61
	2007–2020	7.57 ± 0.71	0.0058 ± 0.0014	13.22 ± 0.76
June	2003–2006	9.73 ± 0.57	0.0053 ± 0.0012	13.20 ± 0.42
	2007–2020	9.53 ± 0.95	0.0077 ± 0.0018	13.50 ± 0.86

* $(x \pm s)$: x represents the mean value and s represents the standard deviation.

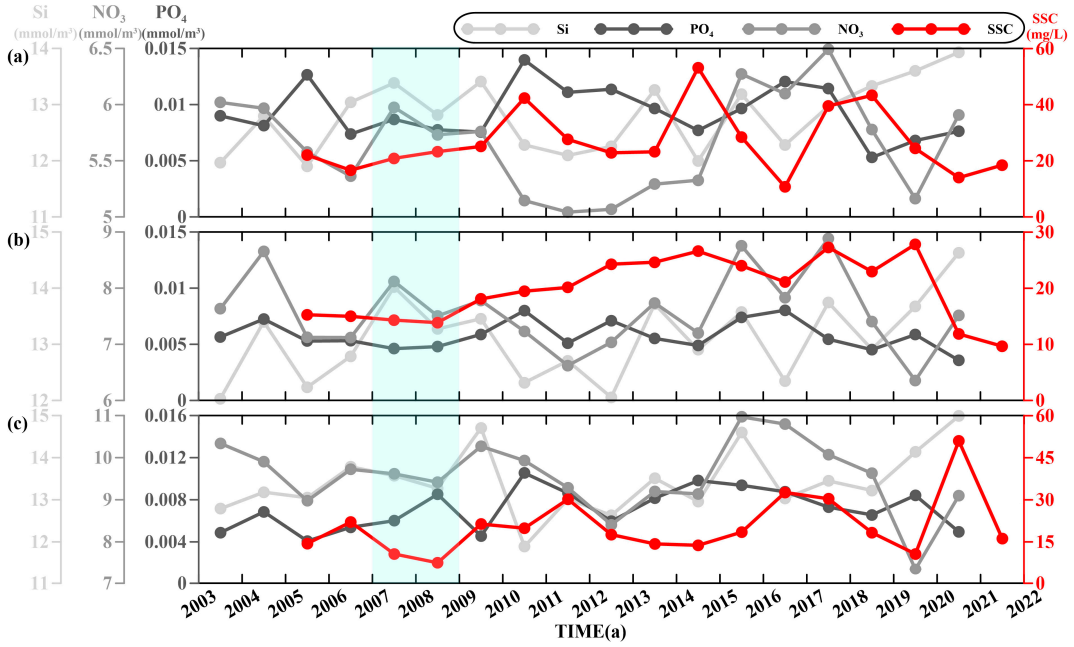

Figure 3. Diagram illustrating nutrient concentration and Suspended Sediment Concentration (SSC) from different months. Blue box indicates the period of the sudden large-scale bloom of *U. prolifera* in 2007–2008. (**a**) April. (**b**) May. (**c**) June.

4.1.2. SST

Following the processing of MODIS/AQUA data, the inversion of the SST, and the computation of PPMCC values, the spatial patterns of PPMCC between SST and *U. prolifera* in different time periods were derived (Figure 4). Prior to early May, *U. prolifera* occurrences are sporadic, making it challenging to calculate its coverage area accurately. By mid-May, the scale of *U. prolifera* starts to become more pronounced, although the PPMCC values for its coverage area are consistently negative. However, a certain positive correlation is observed in the area influenced by the YEWC. In late May, the PPMCC values increase markedly, particularly in the western SYS, reaching 0.5 in most areas. Coastal regions in NJ and the NJNC area, where *U. prolifera* originates, exhibit PPMCC values exceeding 0.75. By early June, there is a positive correlation between SST and the coverage area of *U. prolifera* throughout the SYS. However, from mid-June to late June, when *U. prolifera* generally reaches its MCA, the overall PPMCC values drop below 0.5. The maximum PPMCC value in the central SYS during this period is 0.618. In July, *U. prolifera* gradually

disappears from the southern coast of the Shandong Peninsula, resulting in a predominantly negative correlation with SST. Therefore, from mid-May to late May, the YEWC and the NJNC contribute to the warming of the source area of *U. prolifera*, creating favorable SST conditions for its early growth.

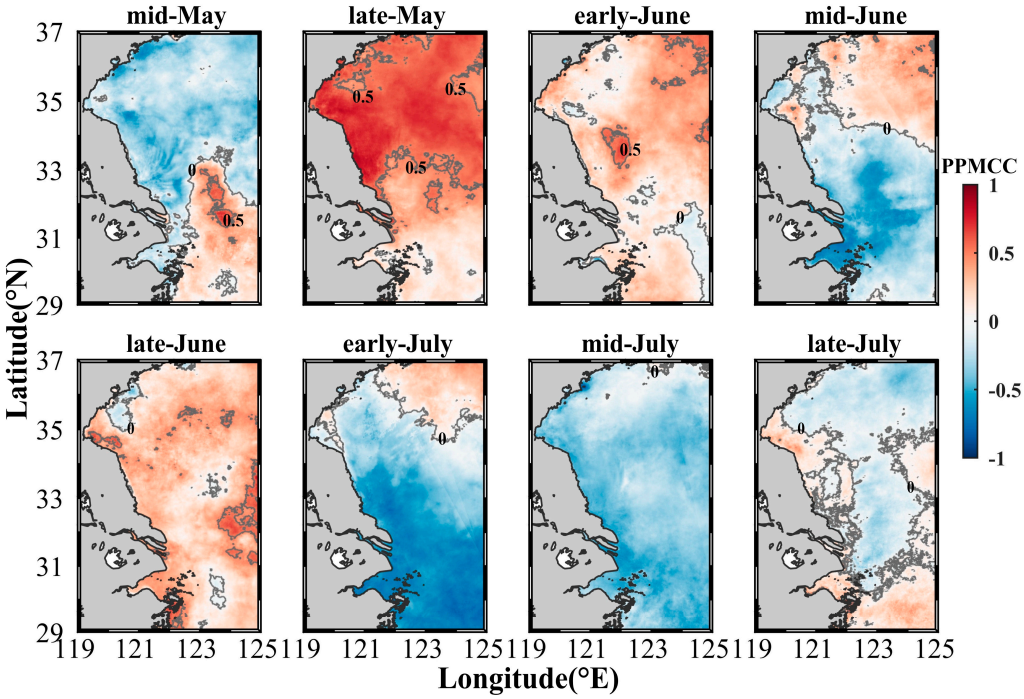

Figure 4. Spatial pattern of the Pearson product-moment correlation coefficient (PPMCC) between SST and the coverage area of *U. prolifera* from mid-May to late July.

4.2. SST Structure Derived from MODIS/AQUA

4.2.1. SST Structure Changes Before and Since 2007

Based on the processing of MODIS/AQUA data and the inversion of the SST, it is possible to derive the spatial pattern of the mean SST structure for different time periods (Figure 5), specifically 2003–2006 and 2007–2022. The main current systems in the SYS (black single-arrow dashed curves in Figure 1) were primarily determined based on previous studies [27–29] and the temperature structure (Figure 5). This study does not consider the SST in August as it exceeds the suitable temperature range for the growth of *U. prolifera* in the entire SYS region.

Figure 5 indicates that the SST structure in the SYS is primarily influenced by the YEWC, NJNC, YSCC, and Yellow Sea warm current (YSWC). From 2003–2006, the middle region of the SYS is strongly influenced by the YSCC, which hinders the northward extension of the YEWC and the NJNC from early April to early May. However, from mid-May onward, as the YSCC and YSWC weaken, the southeast extension of the YSCC retreats toward the coastline. Consequently, the influence of the YEWC and NJNC increases markedly, leading to a rapid warming of the overall SYS, with temperatures exceeding 15 °C. During this period, the YEWC mainly extends northwestward in the northern region of the Yangtze River Estuary. Additionally, the north-east branch (NEB) of the YEWC emerges following the intensification of the Yangtze River Plume in summer [39]. By early June, the YSCC has dissipated, and the SST in the SYS is primarily governed by the NJNC and YEWC. Notably, the influence area of the NJNC gradually extends northward, reaching 36°N by mid-July.

In the period from 2007–2022, the SST during all periods is higher than in the period 2003–2006 (Figure 5). NJNC experiences a notable enhancement in this period, reaching as far north as 36°N in early April. The retraction of the YSWC and YSCC toward the shore

occurs earlier, specifically in early May, weakening their blocking effect on the northward intrusion of YEWC and allowing for its enhanced northwestward extension. From June to July, the YSCC disappears, and the SST in the SYS is primarily influenced by the NJNC and YEWC, similar to the conditions observed during the 2003–2006 period. Additionally, there has been a notable change in the path of the YSCC since 2007, with the main axis shifting eastward. This corresponds to the strengthening of the NJNC, further influencing the SST distribution in April.

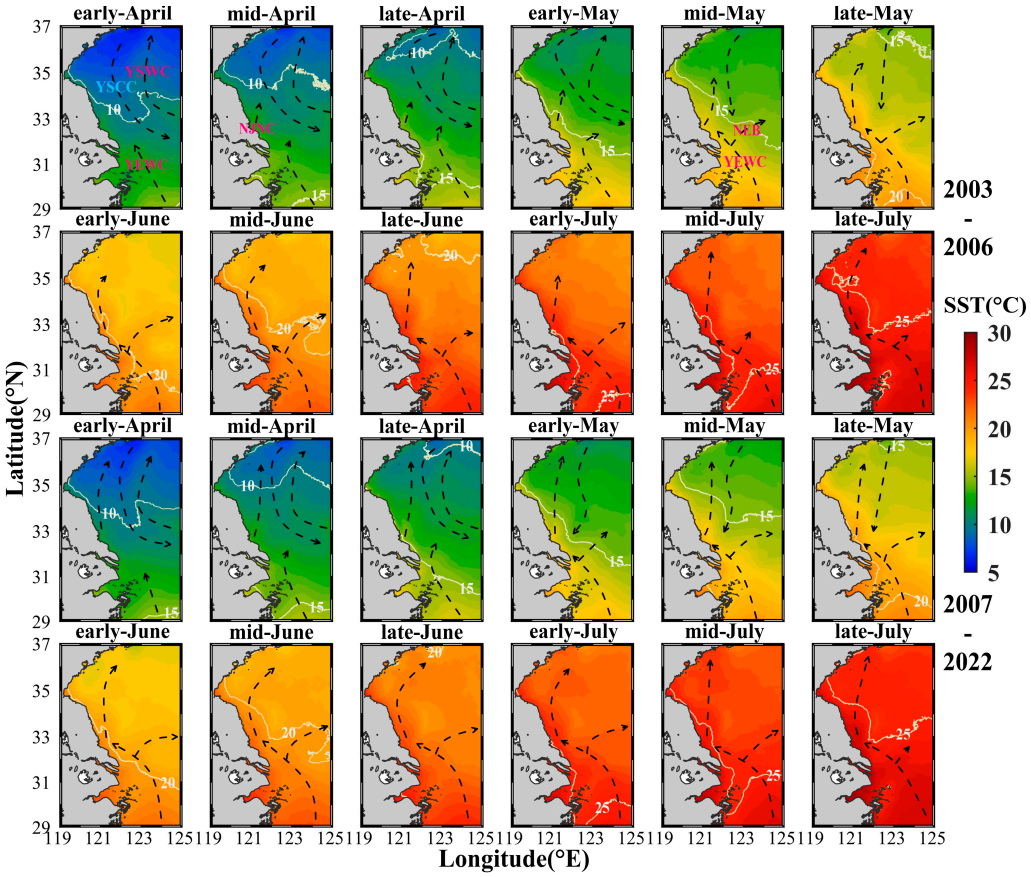

Figure 5. Spatial pattern of SST structure in the Southern Yellow Sea (SYS) from April–July. The black single-arrow dashed curves represent the primary current paths within the SST structure spatial pattern.

The results demonstrate the differences in the SST structure of the SYS from 2003–2006 and from 2007–2022. Following 2007, the increased YEWC and NJNC, characterized by an earlier northward invasion and larger impact area, contribute to a rapid expansion of the *U. prolifera* source area in NJ before mid-May. This region experiences suitable SST conditions for the early development and rapid growth of *U. prolifera*, acting as the key trigger for its large-scale bloom.

4.2.2. Changes in Different *U. prolifera* Bloom Cases

Initially, both the MCA and MDA were subjected to standardized calculations, followed by the application of quadrant segmentation to the functions derived from the MCA and MDA (Figure 2c). The standardized value was calculated using Equation (5) in Table 1.

The *U. prolifera* event exhibits notable interannual variations in bloom time and scale, which can be attributed to environmental changes and human interventions [40]. Thus, it is imperative to classify the intensity of the *U. prolifera* blooms. It is evident that 2009 and 2021 fall within the first quadrant, characterized by substantial-scale blooms. Correspondingly, in the fourth quadrant, two points with the maximum distance from the two points in the

first quadrant, i.e., the points exhibiting the highest dissimilarity, can be identified, i.e., 2012 and 2020 are characterized by minor-scale blooms. Therefore, three typical bloom cases are delineated (Table 3), including the years devoid of *U. prolifera* occurrences from 2003–2006.

Table 3. Typical bloom cases of *U. prolifera*.

Case 1: No *U. prolifera*	Case 2: Minor-Scale (MDA Is Less Than 20,000 km^2 and MCA Is Less Than 500 km^2)	Case 3: Substantial-Scale (MDA Is Greater Than 50,000 km^2 and MCA Is Greater Than 1500 km^2)
2003–2006	2012, 2020	2009, 2021

Based on the average values during the same time periods across years within the same case, the spatial patterns of WR from early April to mid-May and from mid-May to late June of different *U. prolifera* bloom cases are obtained (Figure 6). During the early April to mid-May period, the WRs of the three typical bloom cases exhibit higher values near the coast than in the open sea, primarily influenced by the YSCC. The YEWC and NJNC also display high WR values. However, from mid-May to late June, the WR near the coast becomes lower than that in the open sea.

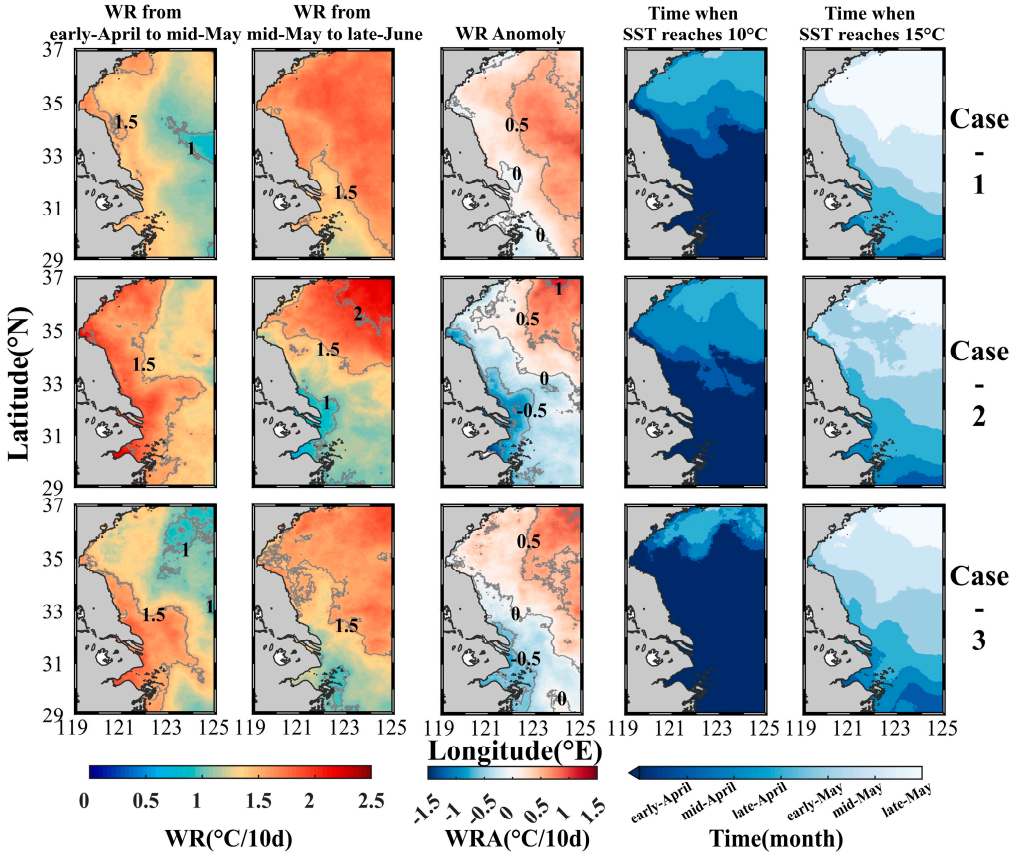

Figure 6. Spatial pattern of SST structure characteristics. Case 1: Period from 2003–2006, characterized by the absence of *U. prolifera* blooms. Case 2: The years of 2012 and 2020, characterized by small-scale blooms of *U. prolifera*. Case 3: The years of 2009 and 2021, characterized by large-scale blooms of *U. prolifera*. The warming rate anomaly (WRA) is calculated by subtracting the warming rate (WR) index from early April to mid-May from that of mid-May to late June for each respective case.

Notably, there is a difference in WR before and after mid-May when comparing Case 1 with Case 2 and Case 3. Therefore, the WRA is calculated in the different areas. Affected by the YEWC and NJNC, Case 1 exhibits a small positive anomaly. In contrast, Case 2 and Case 3 display clear negative anomalies, particularly Case 2, where the anomaly exceeds −0.5 °C/10 d at the Yangtze River estuary and the NJ shallow.

However, when calculating the SST WR, the initial SST (in early April) influences the results. For Case 2, despite having a smaller scale *U. prolifera* bloom than Case 3, the WR is higher before mid-May. Moreover, the area over which WR exceeds 1.5 °C/10 d extends northward to the southern coast of the Shandong Peninsula, rather than being limited to the NJ shallow. Previous studies have shown that early development of *U. prolifera* is initiated when SST reaches 10 °C and large-scale reproduction occurs when SST reaches 15 °C [19]. From the spatial patterns of the time when SST reaches 10 °C and 15 °C for each case (Figure 6), it is evident that SST reaches 10 °C notably earlier in Case 3 than in Case 1 and Case 2. At the time when SST reaches 10 °C, both the YSCC and YSWC play marked roles. For Case 1, in particular, the influence area of the YSCC is between 35°N and 36°N, closer to the shore than in Case 2 and Case 3, resulting in a stronger effect. In contrast, the NJNC only exhibits a noticeable influence area in Case 2 and Case 3. The SST reaches 15 °C at similar times in Case 2 and Case 3, and is notably earlier than in Case 1.

4.2.3. Multi-Year SST Along the Main Current Systems

To investigate the timing and causes of these SST structure changes, square areas with a spatial resolution of 0.5° × 0.5° were selected along the main axes of YEWC, NEB, NJNC, and YSCC (Figures 1 and 5, and Table 4). This study investigated the annual distribution of SST structures and the influence extents of current systems since 2003. This was undertaken to ensure that the selected regions effectively encapsulate the distinctive variations characterizing each current system. By calculating the WRA from early April to mid-May and from mid-May to late June, we obtained a measure of the WR difference during these two time intervals (Figure 7).

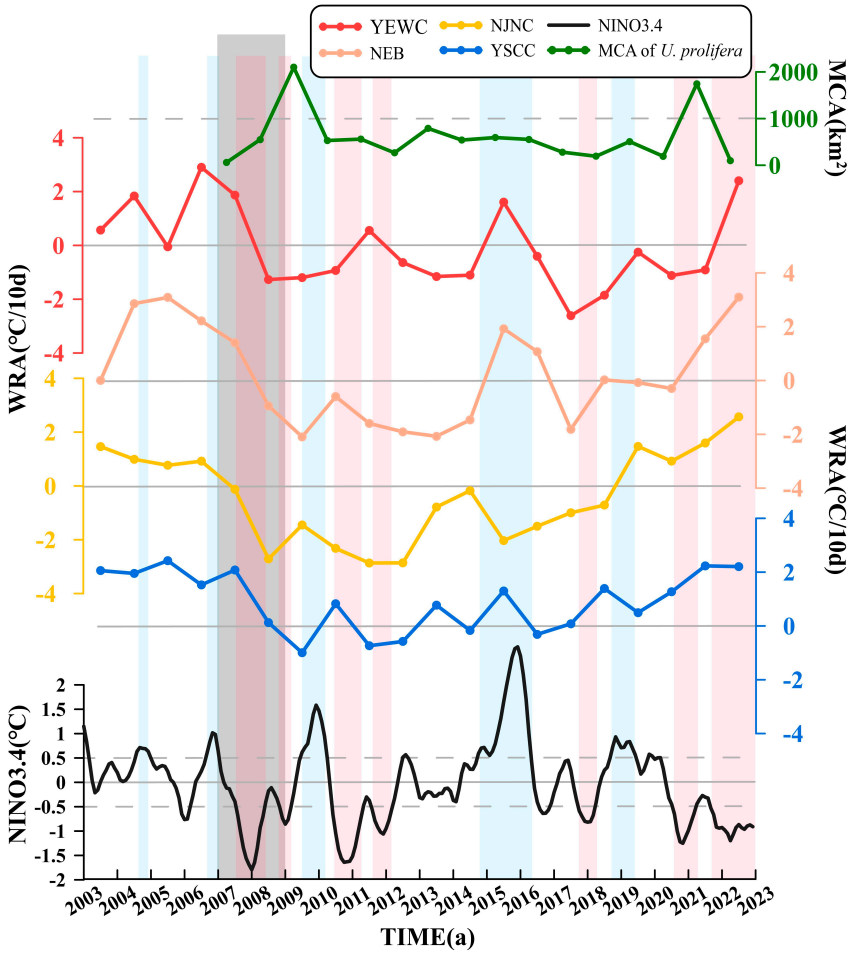

Figure 7. Black curve represents the continuous change in the three-month moving average of the NINO3.4 index from 2003–2022, which is an indicator of El Niño-Southern Oscillation (ENSO) activity.

Green curve represents the maximum coverage area (MCA) of U. prolifera, indicating the extent of U. prolifera blooms. Other curves represent the WRA from early April to mid-May and from mid-May to late June of each year, respectively, as calculated using (3). Blue box indicates an El Niño event, red box indicates a La Niña event.

Table 4. Square area of the main axis of the current system.

Current System	Latitude Range (°N)	Longitude Range (°E)
Warm current across the Yangtze River estuary (YEWC)	30.5–31	123–123.5
Northeast branch (NEB) of YEWC	32.5–33	123–123.5
Northern Jiangsu northward current (NJNC)	33.5–34	121–121.5
Yellow Sea coastal current (YSCC)	33–33.5	122.2–122.7

According to the curves in Figure 7, the WRA values for all current systems undergo a transition from positive to negative during 2007–2008 (gray box in Figure 7). The WRA of the YEWC exhibits a marked change around 2007–2008. Prior to 2008, the SST warms up faster from mid-May to late June (indicating a higher WR). However, after 2008, there is a shift, and the SST starts warming faster from early April to mid-May. This change suggests that, since 2008, the YEWC has contributed to an overall earlier increase in SST in the SYS region. The WRA of the NEB also changes from positive to negative in 2008, indicating a shift in the WR. After 2008, the WR becomes higher from early April to mid-May. This suggests that, although the spatial appearance of NEB is influenced by the intensification of the Yangtze River Plume in June [39], its SST structure is still primarily influenced by the main body of the YEWC. In summary, the changes observed in both the YEWC and NEB indicate that the SST structure in these regions is mainly influenced by the YEWC, with a notable shift occurring around 2007–2008. Additionally, starting from 2007, the WRA of the NJNC from early April to mid-May surpasses that from mid-May to late June. This characteristic remains consistent throughout the period 2007–2018. Both the YEWC and its NEB experience a resurgence in 2015. Furthermore, the influence area of the NJNC corresponds to the source region of *U. prolifera*, directly affecting its early growth. The WRA changes in the NJNC exhibit a closer correspondence to the MCA than the other currents. In terms of the YSCC, this generally indicates a higher WR from mid-May to late June. However, there is a decrease in WRA to a low value in 2008, suggesting that the YSCC plays a stronger role in slowing WR before mid-May than after mid-May. From June onward, the YSCC gradually weakens and eventually disappears, making it difficult to impede the northward intrusion of the YEWC and NJNC. As a result, the overall SYS experiences a rapid warming in SST.

5. Discussion

While the occurrence of green tide events closely relates to multiple factors [8], previous studies [15–17] and the results presented above indicate that nutrient concentration and SSC exhibit a minor variation around 2007–2008 and their correlations with *U. prolifera* are negligible in the SYS. Moreover, the significant increase in PO_4 levels in June primarily observed since 2010 further supports the conclusion that it was not the cause of the 2007 sudden large-scale bloom of *U. prolifera*.

Conversely, the intensity of *U. prolifera* blooms is highly correlated with SST, especially marked by a discernible shift in 2007–2008. Therefore, in this Chapter, we focus on discussing the impact of SST on the 2007 sudden large-scale bloom of *U. prolifera*.

5.1. Response of U. prolifera to SST Variations in the SYS Under Global Changes

Previous studies have indicated that the western Pacific Ocean is particularly susceptible to La Niña events, during which the region experiences elevated temperatures [41,42]. In consideration of the potential influence of global warming on the observed upward trend in SST within the current systems of the SYS over the past two decades, the NINO3.4

index provides a standardized measure to characterize global changes [43]. The NINO3.4 index represents the regional mean SST anomaly within the NINO3.4 region (170–120°W, 5°S–5°N). Its mean value was calculated based on data collected from 1981–2010. To identify El Niño and La Niña events, the *Identification method for El Nino/La Nina events* (GB/T33666-2017, https://openstd.samr.gov.cn/bzgk/gb/index, Accessed on 25 February 2023) was employed [44,45]. According to this method, an El Niño event is determined when the 3-month moving average of the NINO3.4 index exceeds 0.5 °C for a minimum duration of five months. Conversely, a La Niña event is identified when the 3-month moving average falls below −0.5 °C. Analyzing the frequency of El Niño/La Niña events since 1982 (Table 5), it is evident that the occurrence of La Niña events increases sharply from 0.32 to 0.44 between the years 2007 and 2022.

Table 5. Statistics of El Niño/La Niña events.

	No Events (Frequency)	**El Niño (Frequency)**	**La Niña (Frequency)**
1982–2006	7 (0.28)	10 (0.40)	8 (0.32)
2007–2022	4 (0.25)	5 (0.31)	7 (0.44)

On a larger timescale, the two notable temperature structure variations that occurred after 2007 are closely associated with El Niño/La Niña events, specifically during the periods 2007–2011 and 2015–2016 (Figure 7). In the 2007–2011 period, the NINO3.4 index exhibits substantial fluctuations, with a notably high occurrence of strong events, leading to prolonged global climate impacts [44]. In particular, the occurrence of the exceptional La Niña event in 2008 corresponds to changes in the SST structure within the SYS during 2007–2008. This event corresponds to the rapid warming stage of each current system shifting from after mid-May to before mid-May. Between 2012 and 2014, no El Niño/La Niña events were observed, resulting in a renewed elevation of WRA in the NJNC. During the super El Niño event in 2015, the WRA of the YEWC and its NEB experienced a renewed elevation.

Following 2016, the NINO3.4 index exhibits a notable decrease in volatility, and the frequency of El Niño/La Niña events returns to a more typical pattern. Concurrently, the WRAs within each current system demonstrate an upward trend, resembling the conditions observed prior to 2007. This trend is particularly evident for the YEWC, its NEB, and the NJNC. Hence, both the MCA and MDA of *U. prolifera* display a declining trend; the exception is the extensive *U. prolifera* bloom in 2021, which was triggered by a typhoon in May that led to a large influx of breeding rafts into the open sea [46]. The MCA notably decreases to less than 510 km^2, in contrast to the 2100 km^2 observed in 2009. This observation further underscores the impact and role of global changes in *U. prolifera* events.

5.2. Impact Factors of the 2007 Sudden Bloom of U. prolifera

The cultivation of *Porphyra yezoensis* along the NJ shallow dates back to the 1990s, with a sharp increase in its area observed since 2003. This increase creates favorable conditions for the attachment of *U. prolifera* to *Porphyra yezoensis* rafts [7]. However, there were no notable blooms or large-scale spread observed before 2007. Since its initial discovery in the waters of the SYS in 2007, *U. prolifera* has bloomed consecutively for 16 years [8]. The characteristic area parameter known as MCA (Figure 7, green curve), demonstrates substantial peaks in bloom intensity in the years 2009 and 2021, each exceeding 1000 km^2. Notably, since 2010, the MCA has exhibited a certain periodicity with a cycle of 3–4 years. While the *U. prolifera* biomass has been taken into account [24], it presents some differences from the bloom intensity as represented by the MCA. However, the available data in this paper are currently insufficient to facilitate a comprehensive discussion on these discrepancies.

Nevertheless, the reasons behind the 2007 sudden bloom and subsequent large-scale blooms in 2008 were previously unexplained. Based on the results and discussion above, the occurrence of *U. prolifera* events can be attributed to changes in the temperature structure within the SYS region under the influence of global climate change. The WRA values for all current systems undergo a transition from positive to negative during 2007–2008 (gray box in Figure 7). When there are sharp fluctuations in the global climate, particularly with a high frequency of strong El Niño/La Niña events, the SST structure within the SYS undergoes changes [3,47]. This leads to the early appearance of the YEWC and NJNC, occurring before mid-May and impacting a wider area. Consequently, the WR accelerates from early April to mid-May, surpassing the temperature rise observed from mid-May to late June (Figure 6). These conditions provide a more favorable SST environment for the initiation and early growth of *U. prolifera* and are the key factor in the 2007 sudden bloom of *U. prolifera* and its subsequent large-scale blooming since 2008.

The intense and prolonged La Niña event in 2007–2008 obviously influenced the temperature structure changes [48]. Conversely, when the global climate is relatively stable, the temperature structure within the SYS tends to return to its pre-2007 state (Figure 7). The northward intrusion of YEWC and NJNC strengthens after mid-May, which has a negative impact on the scale of *U. prolifera* blooms. Both the 2009 and 2021 *U. prolifera* bloom events in Case 3 occurred after La Niña events. Even the strongest El Niño event in 2015 had only a minor correlation to the scale of the *U. prolifera* event. This suggests that large-scale blooms of *U. prolifera* are more influenced by La Niña events, which increase the likelihood of such blooms occurring. Since the end of 2021, the global climate has been affected by a prolonged La Niña event, although its intensity is not as strong as that of the 2007–2008 event (Figure 7). It has triggered large-scale *U. prolifera* blooms in 2023, with the MCA of 998 km^2, which is the great evidence of the correlation between *U. prolifera* and global climate change.

6. Conclusions

Using MODIS/AQUA data and the GOBAF dataset covering the timeframe from 2003–2022, this study has analyzed the impact of SST, nutrient concentration, and SSC on *U. prolifera*. By integrating the influence of global changes, an investigation into the reasons behind the 2007 sudden bloom has been undertaken. The following conclusions can be drawn.

(1) Nutrient concentration and light intensity have only a minor correlation with *U. prolifera* in the SYS, with the maximum PPMCC values being 0.19 and −0.16, respectively. Instead, the occurrence and intensity of *U. prolifera* events in the SYS are primarily determined by the SST structure, as influenced by the current systems. Coastal regions in NJ and the NJNC area, where *U. prolifera* originates, exhibit PPMCC values exceeding 0.75. Due to the limited availability of in-situ data, further studies may require more extensive discussion of these factors.

(2) Changes in the SST structure serve as a pivotal trigger for the subsequent large-scale bloom of *U. prolifera* after 2007. Notable differences in the SST structure in the SYS exist between the periods 2003–2006 and 2007–2022. During the latter period, there is a marked increase in the intensity of the YEWC and NJNC. These current systems exhibit greater magnitudes and earlier northward invasion times, and cover larger areas. As a result, the WR in the *U. prolifera* source area accelerates before mid-May, particularly in NJ, where the SST becomes conducive to the early development and rapid growth of *U. prolifera*. Since 2008, the time at which the SST reaches 10 °C, a temperature suitable for *U. prolifera* to bloom, has emerged as a critical factor influencing the final scale of *U. prolifera* events. The earlier the SST reaches this threshold, the larger the eventual scale of the *U. prolifera* bloom tends to be.

(3) Since 2007, the changes in the SST structure in the SYS (where *U. prolifera* originates) can be attributed to the impact of global climate change. During the period 2007–2011, there were obvious fluctuations in the global climate, characterized by a high frequency of

intense El Niño/La Niña events. In particular, the intense and prolonged La Niña event from 2007–2008 resulted in alterations in the SST structure in the SYS. In this context, the NJNC directly influenced the *U. prolifera* source area, and its earlier northward intrusion contributed to the occurrence of *U. prolifera* events in 2007–2008. Subsequently, from 2016 onwards, the global climate exhibited a trend towards stabilization, and the temperature structure in the SYS gradually returned to the state observed before 2007. Consequently, the scale of *U. prolifera* events decreased during this period. Since the end of 2021, the global climate has been influenced by a prolonged La Niña event. Although its intensity is not as strong as that observed in 2007–2008, it is still triggered large-scale *U. prolifera* blooms in 2023, with the MCA of 998 km^2, which is the great evidence of the correlation between *U. prolifera* and global climate change.

Author Contributions: Y.P. and P.L. contributed to conception and design of the study. L.X., D.Y. and Q.F. organized the database. Y.P. and J.S. performed the statistical analysis. Y.P. wrote the first draft of the manuscript. P.L., J.S. and S.L. wrote sections of the manuscript. All authors have read and agreed to the published version of the manuscript.

Funding: This research was financially supported by the National Natural Science Foundation of China (grant numbers 42121005) and the Taishan Scholars Project (GXLI). We are also grateful to the editor and anonymous reviewers for their comments and suggestions that have helped us improve the final manuscript.

Data Availability Statement: The raw data supporting the conclusions of this article will be made available by the authors on request.

Acknowledgments: This research was supported by Ocean University of China and First Institute of Oceanography, MNR. We are also grateful to the editor and anonymous reviewers for their comments and suggestions that have helped us improve the final manuscript.

Conflicts of Interest: The authors declare no conflicts of interest.

References

1. Keesing, J.K.; Liu, D.; Fearns, P.; Garcia, R. Inter- and intra-annual patterns of Ulva prolifera green tides in the Yellow Sea during 2007–2009, their origin and relationship to the expansion of coastal seaweed aquaculture in China. *Mar. Pollut. Bull.* **2011**, *62*, 1169–1182. [CrossRef] [PubMed]
2. Li, Y.; Song, W.; Xiao, J.; Wang, Z.; Fu, M.; Zhu, M.; Li, R.; Zhang, X.; Wang, X. Tempo-spatial distribution and species diversity of green algae micro-propagules in the Yellow Sea during the large-scale green tide development. *Harmful Algae* **2014**, *39*, 40–47. [CrossRef]
3. Liu, D.; Keesing, J.K.; Xing, Q.; Shi, P. World's largest macroalgal bloom caused by expansion of seaweed aquaculture in China. *Mar. Pollut. Bull.* **2009**, *58*, 888–895. [CrossRef] [PubMed]
4. Duan, W.; Guo, L.; Sun, D.; Zhu, S.; Chen, X.; Zhu, W.; Xu, T.; Chen, C. Morphological and molecular characterization of free-floating and attached green macroalgae Ulva spp. in the Yellow Sea of China. *J. Appl. Phycol.* **2012**, *24*, 97–108. [CrossRef]
5. Fan, S.; Fu, M.; Wang, Z.; Zhang, X.; Song, W.; Li, Y.; Liu, G.; Shi, X.; Wang, X.; Zhu, M. Temporal variation of green macroalgal assemblage on *Porphyra* aquaculture rafts in the Subei Shoal, China. *Estuar. Coast. Shelf Sci.* **2015**, *163*, 23–28. [CrossRef]
6. Cui, J.; Zhang, J.; Huo, Y.; Zhou, L.; Wu, Q.; Chen, L.; Yu, K.; He, P. Adaptability of free-floating green tide algae in the Yellow Sea to variable temperature and light intensity. *Mar. Pollut. Bull.* **2015**, *101*, 660–666. [CrossRef]
7. Han, H.; Li, Y.; Ma, X.; Song, W.; Wang, Z.; Fu, M.; Zhang, X. Population differentiation in the dominant species (*Ulva prolifera*) of green tide in coastal waters of China. *Acta Oceanol. Sin.* **2022**, *41*, 108–114. [CrossRef]
8. Qi, L.; Hu, C.; Barnes, B.B.; Lapointe, B.E.; Chen, Y.; Xie, Y.; Wang, M. Climate and Anthropogenic Controls of Seaweed Expansions in the East China Sea and Yellow Sea. *Geophys. Res. Lett.* **2022**, *49*, e2022GL098185. [CrossRef]
9. Li, M.; Zhang, R.; Hong, M. Marine disaster assessment and management based on weighted Bayesian network. *Ocean Dev. Manag.* **2018**, *35*, 52–59.
10. Xiao, Y.; Zhang, J.; Cui, T. High-precision extraction of nearshore green tides using satellite remote sensing data of the Yellow Sea, China. *Int. J. Remote Sens.* **2017**, *38*, 1626–1641. [CrossRef]
11. Song, D. Temporal-Spatial Distribution and Countermeasures Study of Algae Disaster in the Bohai and Yellow Sea Based on Multi-Source Data. Ph.D. Thesis, University of Chinese Academy of Sciences (Yantai Institute of Coastal Zone Research, Chinese Academy of Sciences), Yantai, China, 2019.
12. Sun, X. Spatial and Temporal Variations and Response Mechanism of Green Tide and Chlorophyll-a Concentration. Master's Thesis, Ludong University, Yantai, China, 2018.

13. Zhang, G.; Wu, M.; Sun, X.; Zhao, D.; Xing, Q.; Liang, F. The inter-annual drift and driven force of *Ulva prolifera* bloom in the southern Yellow Sea. *Oceanol. Limnol. Sin.* **2018**, *49*, 1084–1093. [CrossRef]
14. Zhang, Z. Obsearvation and Analysis of the Coastal Current and Its Adjacent Current System in the China Offshore Waters. Ph.D. Thesis, Ocean University of China, Qingdao, China, 2016.
15. Shi, X.; Qi, M.; Tang, H.; Han, X. Spatial and temporal nutrient variations in the Yellow Sea and their effects on *Ulva prolifera* blooms. *Estuar. Coast. Shelf Sci.* **2015**, *163 Pt A*, 36–43. [CrossRef]
16. Wang, C.; Chen, C.; Su, R.; Luo, Z.; Mao, L.; Zhang, Y. Mechanism for the marked increase of *Ulva prolifera* in the south Yellow Sea: Light intensity, nitrogen, phosphorus, or co-limitations? *Mar. Ecol.-Prog. Ser.* **2021**, *671*, 97–110. [CrossRef]
17. Bai, Y.; Zhao, L.; Liu, J. The role of ecological factors in the progress of the green tide in the Yellow Sea. *Haiyang Xuebao* **2019**, *41*, 97–105. [CrossRef]
18. Hu, C.; Li, D.; Chen, C.; Ge, J.; Muller-Karger, F.E.; Liu, J.; Yu, F.; He, M.-X. On the recurrent *Ulva prolifera* blooms in the Yellow Sea and East China Sea. *J. Geophys. Res.-Ocean.* **2010**, *115*, C05017. [CrossRef]
19. Yu, Y.; Lin, J.; Jiang, J.; Hu, S.; Kang, C.-K.; Xu, N.; Li, Y. Environmental history affects the growth and photosynthesis of a green-tide macroalgae *Ulva prolifera*. *Aquac. Res.* **2022**, *53*, 2509–2517. [CrossRef]
20. Song, W.; Peng, K.; Xiao, J.; Li, Y.; Wang, Z.; Liu, X.; Fu, M.; Fan, S.; Zhu, M.; Li, R. Effects of temperature on the germination of green algae micro-propagules in coastal waters of the Subei Shoal, China. *Estuar. Coast. Shelf Sci.* **2015**, *163 Pt A*, 63–68. [CrossRef]
21. Sun, X.; Wu, M.; Xing, Q.; Song, X.; Zhao, D.; Han, Q.; Zhang, G. Spatio-temporal patterns of *Ulva prolifera* blooms and the corresponding influence on chlorophyll-a concentration in the Southern Yellow Sea, China. *Sci. Total Environ.* **2018**, *640–641*, 807–820. [CrossRef]
22. Bao, M.; Guan, W.; Yang, Y.; Cao, Z.; Chen, Q. Drifting trajectories of green algae in the western Yellow Sea during the spring and summer of 2012. *Estuar. Coast. Shelf Sci.* **2015**, *163 Pt A*, 9–16. [CrossRef]
23. Son, Y.B.; Choi, B.; Kim, Y.H.; Park, Y. Tracing floating green algae blooms in the Yellow Sea and the East China Sea using GOCI satellite data and Lagrangian transport simulations. *Remote Sens. Environ.* **2015**, *156*, 21–33. [CrossRef]
24. Hu, L.; Hu, C.; Ming-Xia, H.E. Remote estimation of biomass of *Ulva prolifera* macroalgae in the Yellow Sea. *Remote Sens. Environ.* **2017**, *192*, 217–227. [CrossRef]
25. Pan, Y.; Ding, D.; Li, G.; Liu, X.; Liang, J.; Wang, X.; Liu, S.; Shi, J. Potential Temporal and Spatial Trends of Oceanographic Conditions with the Bloom of *Ulva prolifera* in the West of the Southern Yellow Sea. *Remote Sens.* **2021**, *13*, 4406. [CrossRef]
26. Zhang, X.; Zhang, Z.; Lan, X.; Li, R. *Nan Huang Hai Qu Yu Di Zhi*; China Ocean Press: Beijing, China, 2013.
27. Li, G.; Qiao, L.; Dong, P.; Ma, Y.; Xu, J.; Liu, S.; Liu, Y.; Li, J.; Li, P.; Ding, D.; et al. Hydrodynamic condition and suspended sediment diffusion in the Yellow Sea and East China Sea. *J. Geophys. Res. Ocean.* **2016**, *121*, 6204–6222. [CrossRef]
28. Luo, Z.; Zhu, J.; Wu, H.; Li, X. Dynamics of the Sediment Plume Over the Yangtze Bank in the Yellow and East China Seas. *J. Geophys. Res.-Ocean* **2017**, *122*, 10073–10090. [CrossRef]
29. Liu, Z.; Gan, J.; Hu, J.; Wu, H.; Deng, Y. Progress on circulation dynamics in the East China Sea and southern Yellow Sea: Origination, pathways, and destinations of shelf currents. *Prog. Oceanogr.* **2021**, *193*, 102553. [CrossRef]
30. Zhu, P.; Wu, H. Origins and transports of the low-salinity coastal water in the southwestern Yellow Sea. *Acta Oceanol. Sin.* **2018**, *37*, 1–11. [CrossRef]
31. Sun, X. *Zhong Guo Jin Hai Qu Yu Hai Yang*; China Ocean Press: Beijing, China, 2006.
32. Qiao, F.; Wang, G.; Lü, X.; Dai, D. Drift characteristics of green macroalgae in the Yellow Sea in 2008 and 2010. *Chin. Sci. Bull.* **2011**, *56*, 2236–2242. [CrossRef]
33. Li, Y. *Structure and Dynamics of Ocean Circulation off the East Coast of China*; Chinese Academy of Sciences: Beijing, China, 2010.
34. Wen, S.; Song, X.; Tian, Y.; Zhang, Q.; Chen, C.; Gao, S.; Zhao, D. Technology and method for economic losses assessment of red tide disasters. *J. Catastrophol.* **2015**, *30*, 25–28. [CrossRef]
35. Xie, X.; Tao, A.; Zhang, Y.; Zeng, Y.; Zheng, J. The temporal and spatial distribution characteristics of typical marine disasters in Fujian Province. *Trans. Oceanol. Limnol.* **2018**, *4*, 21–30. [CrossRef]
36. He, E.; Ji, X.; Huang, H.; Wang, D.; Guo, M.; Gao, S.; Yang, J. The spatial and temporal distribution of *Ulva prolifera* in the Yellow Sea in recent 10 years. *Mar. Forecast.* **2021**, *38*, 1–11. [CrossRef]
37. Zhang, M.; Tang, J.; Dong, Q.; Song, Q.T.; Ding, J. Retrieval of total suspended matter concentration in the Yellow and East China Seas from MODIS imagery. *Remote Sens. Environ.* **2010**, *114*, 392–403. [CrossRef]
38. Zhang, L.; Qiao, L.; Zhong, Y.; Li, G.; Liu, Y. Alternating patterns of cross-shelf suspended sediment transport in the northern East China Sea in winter. *Mar. Geol.* **2023**, *463*, 107114. [CrossRef]
39. Zhang, Z.; Chen, Y.; Luo, F. Temporal and spatial distribution characteristics of Enteromorpha prolifera in the South Yellow Sea based on remote sensing data of 2014. *J. Huaihai Inst. Technol.* **2016**, *25*, 80–85. [CrossRef]
40. Xia, Z.; Yuan, H.; Liu, J.; Sun, Y.; Tong, Y.; Zhao, S.; Xia, J.; Li, S.; Hu, M.; Cao, J.; et al. A review of physical, chemical, and biological green tide prevention methods in the Southern Yellow Sea. *Mar. Pollut. Bull.* **2022**, *180*, 113772. [CrossRef] [PubMed]
41. Huang, Z.; Du, Y.; Wu, Y.; Xu, H. Asymmetric Response of the South China Sea SST to El Niño and La Niña. *J. Ocean Univ. China* **2013**, *12*, 272–278. [CrossRef]
42. Lin, H. Long-lead ENSO control of the boreal summer intraseasonal oscillation in the East Asian-western North Pacific region. *npj Clim. Atmos. Sci.* **2019**, *2*, 31. [CrossRef]

43. Buchmann, P.; DelSole, T. Week 3–4 Prediction of Wintertime CONUS Temperature Using Machine Learning Techniques. *Front. Clim.* **2021**, *3*, 697423. [CrossRef]
44. Hong, X.; Zhang, K.; Li, J.; Xu, Y.; Sun, M.; Jiang, J.; Xu, S.; Cai, Y.; Qiu, Y.; Chen, Z. Impacts of climate events on life history parameters of major commercial fishes in the Beibu Gulf, South China Sea in the last 15 years. *Front. Mar. Sci.* **2023**, *10*, 1234772. [CrossRef]
45. Fan, J.; Wei, S.; Liu, D.; Qin, T.; Xu, F.; Wu, C.; Liu, G.; Cheng, Y. Impact of ENSO events on meteorological drought in the Weihe River basin, China. *Front. Earth Sci.* **2023**, *11*, 1093632. [CrossRef]
46. Qi, L.; Wang, M.; Hu, C. Uncertainties in MODIS-Derived *Ulva prolifera* Amounts in the Yellow Sea: A Systematic Evaluation Using Sentinel-2/MSI Observations. *IEEE Geosci. Remote Sens. Lett.* **2023**, *20*, 1–5. [CrossRef]
47. Li, Y.; Feng, J.; Yang, X.; Zhang, S.; Chao, G.; Zhao, L.; Fu, H. Analysis of sea level variability and its contributions in the Bohai, Yellow Sea, and East China Sea. *Front. Mar. Sci.* **2024**, *11*, 1381187. [CrossRef]
48. Luo, J.; Behera, S.K.; Masumoto, Y.; Yamagata, T. Impact of Global Ocean Surface Warming on Seasonal-to-Interannual Climate Prediction. *J. Clim.* **2011**, *24*, 1626–1646. [CrossRef]

Disclaimer/Publisher's Note: The statements, opinions and data contained in all publications are solely those of the individual author(s) and contributor(s) and not of MDPI and/or the editor(s). MDPI and/or the editor(s) disclaim responsibility for any injury to people or property resulting from any ideas, methods, instructions or products referred to in the content.